Iranian Journal of Basic Medical Sciences
ijbms.mums.ac.ir

# *In vitro* pro-apoptotic and anti-metastatic potentials of harmaline-silver containing folate-linked chitosan nano-drug delivery system

**Ali Hussein Wannas Al-Harmooshee [1], Masoud Homayouni Tabrizi [2]*, Nasim Hayati Roodbari [2]**

[1] Department of Biology, Science and Research Branch, Islamic Azad University, Tehran, Iran
[2] Department of Biology, Mashhad Branch, Islamic Azad University, Mashhad, Iran

**ARTICLE INFO**

***Article type:***
Original

***Article history:***
Received: Apr 15, 2023
Accepted: Aug 19, 2023

***Keywords:***
Anti-metastatic activity
Apoptotic activity
Cancer-selective-cytotoxicity
Harmaline-ag containing-folate-linked chitosan-nanoparticles (HA-fCNP)

**ABSTRACT**

***Objective(s):*** Harmaline and green-synthesized silver nanoparticles were encapsulated by folate-linked chitosan molecules as a receptor-mediated drug delivery system to evaluate its pro-apoptotic and anti-metastatic potentials on human ovarian (A2780) and epithelioid (PANC) cancer cells.

***Materials and Methods:*** The Ag nanoparticles (AgNP) were synthesized utilizing an herbal bio-platform (Bistorta officinalis) and embedded with harmalin. The Harmaline-ag containing folate-linked chitosan nanoparticles (HA-fCNP) were synthesized utilizing the ionic gelation method. Both the AgNP and HA-fCNP nanoparticles were characterized by DLS, FESEM, and Zeta potential analysis. Moreover, the chemical properties of HA-fCNP and the crystallinity of AgNPs were determined by applying FTIR and XRD methods, respectively. The HA-fCNP cytotoxicity was analyzed on A2780, PANC, and HFF cell lines. Moreover, pro-apoptotic and anti-metastatic potentials of HA-fCNP were studied by analyzing the BAX-BCL2 and MMP2-MMP9 gene expression profiles, respectively. The A2780 cellular death was determined by AO/PI and flow cytometry methods.

***Results:*** The HA-fCNP significantly exhibited a selective cytotoxic impact on A2780 and PANC cancerous cell lines compared with normal human foreskin fibroblast (HFF) cells. The increased SubG1-arrested A2780 cells and up-regulated BAX gene expression following the increased treatment concentrations of hA-fCNP indicated its selective pro-apoptotic activity on A2780 cells. Also, the notable down-regulated expressions of MMP2 and MMP9 metastatic genes following the increasing doses of HA-fCNP treatment on A2780 cells confirmed its anti-metastatic activity.

***Conclusion:*** The cancer-selective cytotoxicity, apoptotic, and anti-metastatic properties of HA-fCNP are considered the appropriate properties of an anticancer compound.

▶ Please cite this article as:
Al-Harmooshee AHW, Homayouni Tabrizi M, Hayati Roodbari N. *In vitro* pro-apoptotic and anti-metastatic potentials of harmaline-silver containing folate-linked chitosan nano-drug delivery system. Iran J Basic Med Sci 2024; 27: 180-187. doi: https://dx.doi.org/10.22038/IJBMS.2023.71731.15602

## Introduction

Among several types of human cancers, ovarian carcinoma is known as one of the most dangerous ones due to its silent carcinogenesis development and high recurrence rate (1, 2). The common ovarian cancer treatment strategies are not selective enough to avoid their clinical side effects (3). Therefore, focusing on the more targeted and selective anticancer compound can be considered one of the main issues in ovarian cancer treatment strategies.

To reach efficient cancer treatment strategies, it is required to review the carcinogenesis process of cancer cells. The transformation of normal cells into cancerous types is mediated by various types of carcinogenic risk factors such as oxidative stress inducers (4). The transformed cancerous cells need to increase their survival under their related metabolic-mediated oxidative stress by down-regulating the apoptosis inducers such as BAX and up-regulating anti-apoptosis effectors such as BCL2.

The produced exogenic reactive oxygen species (ROS) is the main cause of oxidative stress near both the normal and cancerous cells, which acts as both tumor-suppressive and tumor-progressive factors. The excess amount of ROS acts as the tumor-suppressive factor by significantly inducing apoptosis in both normal and cancer cells. Therefore, scavenging the elevated ROS amounts just near the normal cells prevents the cancer transformation process and saves normal cells against ROS-mediated oxidative stresses (5).

On the other hand, the initially caner-mediated secretion of ROS to the cancer microenvironment acts as the tumor progressive factor by inducing local inflammation and calling immune cells to the tumor tissue. Cancer cells recruit the infiltrated macrophages to utilize their powerful secretion system and get ready for migration (6, 7). In this regard, cancer cells increase the expression of MMP2 and MMP9 to facilitate their migration to their next appropriate proximal or distal tissues (8, 9). Therefore, producing the apoptotic, anti-metastatic, and antioxidant compounds has the potential to simultaneously remove cancerous cells and save normal types against the toxic anti-cancer compounds.

Nanotechnology has solved the challenging obstacles in the treatment of ovarian cancer by preparing precise drug delivery and molecular imaging possibilities. The functionalized stable drug nanocarriers such as solid lipid nanoparticles (SLN), liposomes, and polymeric nanoparticles have presented efficient and bio-accessible cancer-selective cytotoxicity in several types of tumors (10-13). Several types of mineral-based compounds such as copper, gold, silver, and selenium nanoparticles have been

*Corresponding author: Masoud Homayouni Tabrizi. Department of Biology, Mashhad Branch, Islamic Azad University, Mashhad, Iran. Email: mhomayouni6@mshdiau.ac.ir

reported as powerful anticancer compounds (14-18). Also, the nano-drug delivery systems have opened a promising horizon for more efficient treatment of ovarian carcinoma by utilizing the encapsulated herbal anticancer compounds such as liposomal genistein (19, 20), encapsulated shikonin nanoparticles (21), liposomal irinotecan/doxorubicin (22), and curcumin-loaded nanoparticles (23).

Moreover, the ovarian cancer cells have been targeted by folic acid-conjugated nano-drug delivery systems consisting of poly (ethylene glycol)-chitosan oligo-saccharide lactate (PEG-COL) nanoparticles (24) and lecithin nanoemulsions (25). The mentioned folic acid-conjugated nano-drug delivery systems have suppressed ovarian cancer proliferation by being selectively accumulated in tumor sites, which verifies the overexpression of membrane folate receptors in ovarian cancer cells (24, 25).

Herein, a mixture of insoluble silver nanoparticles and the herbal extracted harmaline as the two powerful anticancer elements (26, 27) were selected to be encapsulated by folic acid-conjugated chitosan, a natural positive-charged polymer with limited immunogenicity and high degrees of biocompatibility. The anticancer activity of the silver nanoparticles (Ag NPs) have been verified by studying several types of plant-bio-platforms mediating the Ag NPs synthesis including *Taraxacum officinale,* and *Commelina nudiflora L*, which indicated the significant cytotoxic impact on HepG2, and HCT-116 cancer cells, respectively (28, 29). The harmaline-Ag containing folate-linked chitosan nanoparticles (HA-fCNP) were synthesized to investigate their selective apoptotic, and anti-metastatic potentials on human ovarian (A2780) and epithelioid (PANC) cancer cells.

## Materials and Methods

### *Materials*

Harmaline, folic acid (FA), low molecular weight (LMW) chitosan, and acridine orange (AO)/propodium iodide (PI) were prepared from Sigma-Aldrich. The antioxidant free radicals including 2,2′-Azino-bis(3-ethylbenzothiazoline-6-sulfonic acid) (ABTS) and 2,2-diphenyl-1-picrylhydrazyl (DPPH), potassium persulfate, dimethyl sulfoxide (DMSO), and 3-(4,5-dimethylthiazol-2-yl)-2,5-diphenyl-2H-tetrazolium bromide (MTT) were ordered from Merck Co. All the cell culture requirements were purchased from Invitrogen Co. The target cell lines including the ovarian (A2780) and epithelioid (PANC) cancer cell lines were prepared from the cell bank unit of Ferdowsi University of Mashhad, Iran. The abbreviation list is provided in Table 1.

### *AgNP green synthesis*

#### *Bistorta officinalis preparation*

The aqueous extract of *B. officinalis* was utilized for the biosynthesis of AgNPs. Briefly, fresh leaves of *B. officials* were collected, rinsed, and dried at room temperature. The 10 g of cut small pieces of *B. officinalis* leaves were boiled at 80 ˚C for 20 min. The boiled leaves were centrifuged at 12000 rpm for 10 min at 4 ˚C after gradually cooling. The supernatant was applied for AgNP biosynthesis.

#### *AgNP synthesis*

In order to prepare the green-synthesized AgNP nanoparticles, 1 mM concentration of silver nitrate ($AgNO_3$) was embedded with 10 ml of *B. officinalis* leaf extract in a 250 ml Erlenmeyer, mixed by a magnet stirrer at room temperature, and incubated in the dark conditions overnight at 30 ˚C. The colloidal brownish-yellow color of the solution was considered as the complete $AgNO_3$ to $Ag^+$ reduction process. The produced AgNP colloid was used for future use.

### *Preparation of HA-fCNP*

The HA-fCNP was synthesized by applying the ionic gelation method. Briefly, to produce HA-fCNP nanoparticles, first, the chitosan solution (0.2% W/V) was prepared with 2% acetic acid solution and incubated at 60 ˚C for 1 hr under stirring conditions (700 rpm). Then, TPP (1 mg/ml), 2.1 g of harmaline, and 1 g of AgNP were mixed with 100 ml DMSO. Gelation was performed by gradually inserting the prepared mixture into the chitosan gel at the proportion of 3 : 1 under stirring at 700 rpm for 30 min. Finally, the harmaline/Ag-loaded chitosan nanoparticles (HA-CNP) were centrifuged at 4000 rpm and rinsed three times to remove not-encapsulated harmaline-Ag components. The precipitate was resolved in 10 ml of deionized water. Then, the HA-CNP mixture was mixed with 10 mg folic acid solution (5% DMSO V/V) and acetic acid solution (10% V/V) was utilized to adjust the final solution acidity at pH=5. Next, an appropriate volume of EDC (0.01 M) was added drop-wise to the final solution. Finally, the mixture was incubated at 40 °C for 12 hr in a shaker incubator. The HA-fCNP was rinsed three times by centrifuging at 10000 rpm for 10 min, utilizing deionized water.

### *Physicochemical characterization of AgNPs and HA-fCNP*

ζ-potential, Z average, and PDI values of both AgNPs HA-fCNP were measured by DLS methods. In this regard, 1 ml of both AgNPs and HA-fCNP was separately diluted with 10 ml of deionized water and measured at a 175˚ scattering angle at 25±0.5 ˚C. The morphology of both AgNPs and HA-fCNPs was detected by field emission scanning microscopy (FESEM). A 50-µl drop of both diluted AgNPs and HA-fCNP was dried on a soft aluminum foil piece. Then, the gold-coated surface of the sample was prepared for FESEM imaging. The FTIR spectroscopy technique was utilized to study the chemical properties of both AgNPs and HA-fCNP structure including the individual characteristic wavenumbers of its bonds and functional groups by preparing the compressed thin tablets of both AgNPs and HA-fCNP. The tablets were produced by combining 2 mg of HA-fCNP with potassium bromide (KBr).

### *HA-fCNP loading efficiency*

The HA-fCNP's loading efficiency was measured by the UV-visible spectroscopy method. Briefly, the standard curve was plotted by recording harmaline's Uv-visible absorbance peak in its certain concentrations at 350 nm. Then, harmaline's absorbance was recorded before and after the production process by applying a UV-visible spectrophotometer (225 nm). The loading efficiency (LE%) was measured by calculating the harmaline concentration before and after the encapsulation process by the following equation:

$$LE\ \% = (\text{harmaline})\ A\ /(\text{harmaline})\ B \times 100\%$$

### *Cell survival measurement*

The HA-fCNP's toxicity in both A2780 and PNCK cancer cell lines was studied by conducting an MTT assay. For this

purpose, $6\times10^3$ cells/well were seeded on 96-well plates and incubated for 24 hr under standard cell culture conditions. The normal human foreskin fibroblast (HFF) and cancer cell lines were cultured in DMEM (Gibco) and RPMI medium, respectively. The mediums were supplemented with 10% fetal bovine serum (FBS), 100 IU/ml of penicillin, streptomycin (100 µg/ml), and L-glutamine (2 mM). The cells were incubated at 37 ˚C and 95% humidity in 5% carbon dioxide conditions.

The treatment program was initiated after 24 hr of incubation. Different doses of HA-fCNP (0, 15.6, 31.2, 62.5, 125, and 250 µg/ml) were prepared in phosphate buffer (pH=6.8) to be treated and exposed to the cultured cancer cells.

Upon the cells past the 48-hour treatment incubation, the fresh medium supplemented with 0.5 mg/ml MTT dye was replaced by the old medium and incubated for a further 3 hr under standard culturing conditions. Finally, the medium of the wells was re-filled by DMSO (100 µl) and incubated for 15 min. The recorded formazan absorbance at 570 nm reflected the cell survival index. The cell survival rate was calculated by the following equation:

Cell survival rate %=(OD)sample/(OD)control×100

***Gene expression profile***

To evaluate the expression of the metastatic (MMP2 and MMP9), anti-apoptotic (BCL2), and apoptotic (BAX) gene expression, the treated cancer cells were harvested and their total RNA was extracted by applying the Biotech kit. The RNA extraction quality was evaluated by the nanodrop method. The extracted RNAs were used to prepare cDNA libraries utilizing the Pars tous kit. The target gene primer sets were designed using the Allele ID6 software package (Table 2). To measure the target gene expression profile, a comparative Q-PCR was utilized (CFX-96 Bio-Rad) by applying a SYBR green PCR Master Mix (Qiagen, Hilden, Germany) supplemented with ROX reference dye. Finally, the gene expression normalization was conducted by measuring the GAPDH gene expression by applying the comparative threshold cycle method.

***Flow-cytometry***

A2780 cells were cultured and incubated with a range of HA-fCNP concentrations (0, 25, 100, and 175 µg/ml) for 48 hr. The cells were washed with PBS, harvested, fixed with cold ethanol, and re-suspended on 200 µl PI dye (1 mg/ml). The cell suspensions were incubated for 30 min in dark conditions. Finally, the cells' cycle details were analyzed by a FACSacn laser flow cytometer.

***AO/PI double staining***

The apoptotic morphological evidence of A2780 cells was studied by applying the AO/PI staining method. The A2780 cancer cells were treated with a range of HA-fCNP concentrations (0, 25, 100, and 175 µg/ml) for 48 hr. Then, they were fixed with the 4% paraformaldehyde, stained with AO/PI dyes at the proportion of 1:1 and incubated for 15 min at standard conditions. The stained cells were washed, harvested, and fixed with cold ethanol (70%). The stained cells were visualized by UV illumination.

***Scratch assay***

To conduct the scratch analysis, $4\times10^4$ cells were seeded to a 6-well plate and cultured for 24 hr. Then, a thin scratch was created after draining the culture medium by applying a sampler tip. The plates were washed with PBS to remove the separated cells and filled with the fresh cell culture medium. Finally, 25 µ/ml concentration of HA-fCNP was exposed with the scratched culture plate and incubated for 24 hr. The metastasis inhibition rate was estimated as the following equation:

%Inhibition rate=(scratch width after 24 hrs)/(scratch width at the beginning of exposure)×100

## Results

***Characterization of HA-fCNP***

The FESEM imaging technique showed that the AgNP nanoparticles were produced at ~90 nm diameter, which was greater than 2 times smaller than HA-fCNP size (226.83 nm)(Figure 1A). Moreover, DLS supported the reported FESEM size for both AgNPs and HA-fCNP by estimating the 86.4-nm and ~250 nm nanoparticles, respectively. The AgNPs and HA-fCNP were produced with acceptable polydispersity Indexs (PDI) of 0.25 and 0.28, respectively. It has shown been that less than 0.7 PDI values show the mono-distribution phase formation of the nanoparticles, which is reliable enough to be reported as their real dimension (Figure 1B)(30). Also, the estimated zeta potential value of both AgNPs (+25.1 mV) and HA-fCNP (+26.2 mV) nanoparticles indicates their suitable defensive electrostatic interactions, which increase their stability in aqueous solutions. Considering Salopek's studies, the stability of the nanoparticles is decreased in higher than ±20 mV electrostatic charges. Therefore, both the AgNPs and HA-fCNP particles have the potential to be stable as a drug delivery system (Figure 1C)(31).

The crystallinity of AgNPs was verified by detecting the three individual Ag peaks between 30 to 45 degrees (Figure

**Table 2**. The sequence of apoptosis, metastasis and housekeeping genes primer sets

| Target genes | Forward sequence | Reverse sequence |
|---|---|---|
| GAPDH | TGCTGGTGCTGAGTATGTCG | GCATGTCAGATCCACAACGG |
| BAX | GATAACGGAGGCTGGGATGC | TCATTGTGGCCCAGATAGG |
| BCL2 | AAACTGGTGCTCAAGGCCC | CTTCAGTGACTCGGCCAGG |
| MMP2 | CACGCTGGGCCCTGTCACTCCT | TGGGGCCTCGTATACCGCATCAAT |
| MMP9 | TGCCCGGACCAAGGATACAGTTT | AGGCCGTGGCTCAGGTTCAGG |

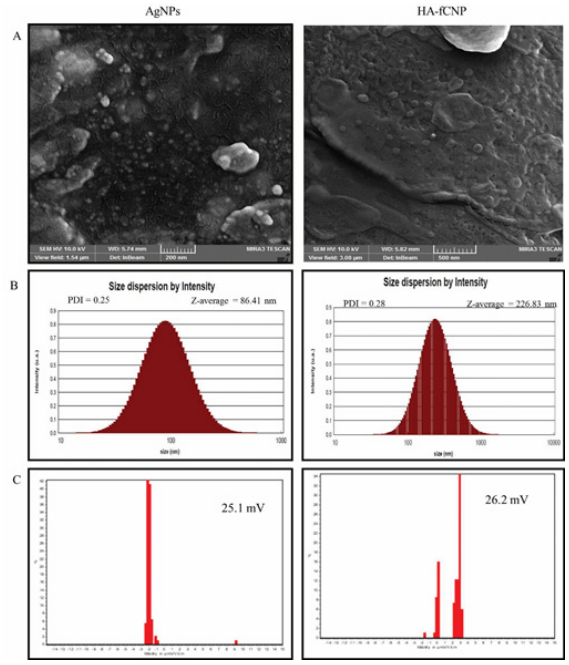


**Figure 1.** Size and particle stability characteristics of HA-fCNP
HA-fCNP: Harmaline-ag containing folate-linked chitosan nanoparticles

2A)(32). Moreover, the FTIR spectrum verified the HA-fCNP structure (Figure 2B). The characteristic peaks of chitosan, harmaline, folic acid, and Ag confirm the success of HA-fCNP formation. The characteristic absorption bands of chitosan have been detected for N-H bending of primary amine at 1654 $cm^{-1}$ and 1571 $cm^{-1}$, and C–N stretching of primary amine at 1026 $cm^{-1}$ (33). Harmaline characteristic absorption bands have been observed for OH-stretching of hydroxyl groups and phenols at 3300 $cm^{-1}$ to 3500 $cm^{-1}$ for both harmaline and silver spectra (34).

### *Loading efficiency of harmaline*

The harmaline loading efficiency was estimated as mentioned in section 2.4. During the encapsulation process, 90.2% of harmaline contents were incorporated into the cationic chitosan polymer molecule.

### *Cytotoxicity of HA-fCNP*

During 48 hr of incubation, HA-fCNP significantly reduced the cell survival rate of A2780 cancer cells by its enhanced treatment concentration compared with other cancer (PANC) and normal (HFF) cell lines (Figure 3). The IC50 concentration of HA-fCNP was estimated at

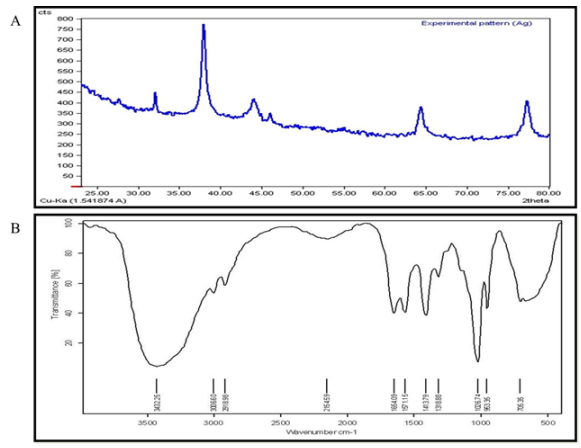


**Figure 2.** XRD (A) and FTIR (B) results of HA-fCNP
HA-fCNP: Harmaline-ag containing folate-linked chitosan nanoparticles

102.73 µg/ml in A2780 cancer cell line. The results show a meaningful association among the cell lines' response to HA-fCNP treatment.

### *Apoptotic and metastatic potential of HA-fCNP*

The cellular death type was determined by studying the cancer cell morphology and cell cycle status following the increasing HA-fCNP treatment doses. The increased shrunk cells following the enhanced treatment concentrations of HA-fCNP indicates the apoptotic dead cells (Figure 4A), which was verified by detecting a significant enhancement in SubG1-arrested cell populations following the high treatment doses of HA-fCNP nanoparticles, which indicates the apoptosis occurrence in treated cells (Figure 4B). The increased cell population in the SubG1 phase from 4.5 to 25.1% was estimated following the increasing HA-fCNP doses up to 25 µg/ml. This is while the high HA-fCNP concentration (175 µg/ml) significantly increases the subG1-arrested cells (76%) and prevents carcinogenesis. In other words, the HA-fCNP cytotoxicity can be attributed to its apoptotic activity.

Moreover, to verify the apoptotic occurrence a further apoptosis assay was designed based on AO/PI cell staining technique. Acridine orange, a vital dye makes the normal alive cells green, and PI penetration into the apoptotic cells produces red points. As shown in Figure 5 the notable enhancement of the red points following the increased HA-fCNP treatment doses indicates the apoptotic PI-penetrated cells.

Finally, to study the HA-fCNP-mediated apoptotic

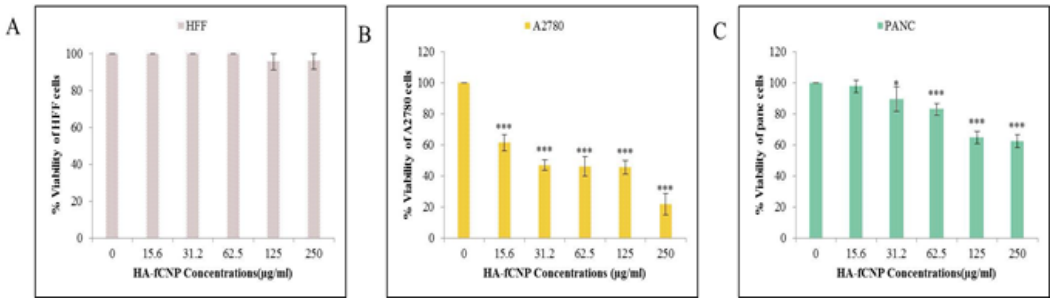


**Figure 3.** HA-fCNP cytotoxic impact on HFF (A), A2780 (B), and PANC (C) cell lines after 48 hr of incubation
HA-fCNP: Harmaline-ag containing folate-linked chitosan nanoparticles; HFF: human foreskin fibroblast; PANC: epithelioid

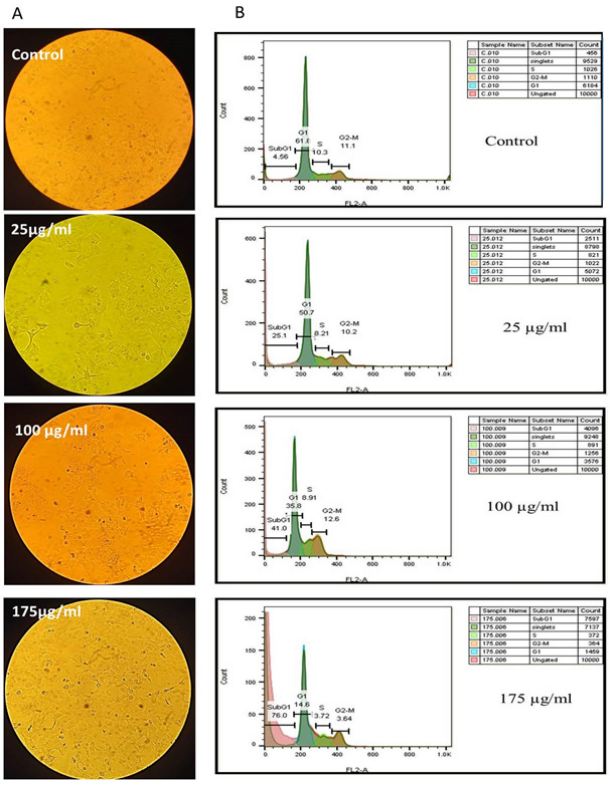


**Figure 4.** A2780 cancer cell death type
A) A2780 cancer cell morphology following the increased HA-fCNP treatment doses.
B) Flow-cytometry analysis of A2780 cancer cells
HA-fCNP: Harmaline-ag containing folate-linked chitosan nanoparticles

mechanism, the expression of BAX and BCL2 genes was analyzed. The result shows a significant up-regulation of BAX and a meaningful down-regulation of the BCL2 gene, which verifies the apoptotic-mediated cytotoxic impact of HA-fCNP (Figure 6).

### *HA-fCNP metastatic potential*

The metastatic potential of HA-fCNP was evaluated by conducting the scratch assay. The not-grown A2780 cells in the scratched-line during 24-hr exposure with 25 µg/ml concentration of HA-fCNP indicated the inhibition rate of metastasis at 75.14% (Figure 7). Moreover, measuring the most important genes of migration required enzymes including MMP2 and MMP9 genes. The results indicate a significant negative association with the increasing HA-fCNP treatment doses on the A2780 cell line (Figure 8). In other words, the HA-fCNP decreases A2780 cells' migration to other proximal and distal cancer niches.

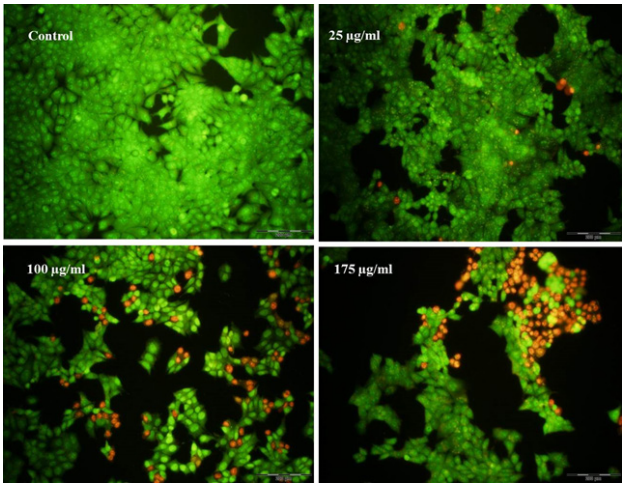


**Figure 5.** AO/PI staining results of A2780 ovarian cancer cells after being treated with a range of HA-fCNP treatment doses
HA-fCNP: Harmaline-ag containing folate-linked chitosan nanoparticles; AO/PI: Acridine orange /propodium iodide

## Discussion

The precise functionalized drug delivery systems have opened a promising horizon for targeted cancer treatment strategies. To the best of our knowledge, this is the first encapsulation of harmaline-silver hybrid nanoparticles by folate-conjugated chitosan polymers and studying their apoptotic and metastatic potentials. The nanoparticles significantly decreased the ovarian A2780 cancer cells by selectively inducing apoptotic-mediated cytotoxic impact compared with normal (HFF) and cancerous (PANC) cell lines. Moreover, they meaningfully down-regulated the cancer migration required enzymes (MMP2 and MMP9) in A2780 ovarian cancer cells and suppressed their metastatic ability.

Normal cells can be transformed into cancerous types following exposure to exogenous- or endogenous-oxidative stress mediated by reactive oxygen species (ROS). The mild compensable oxidative stress inactivates the cell tumor suppressors. The mutated tumor suppressor genes facilitate cancer cell high-rate proliferation by allowing them to unlimitedly pass cell cycle checkpoints (4). On the other

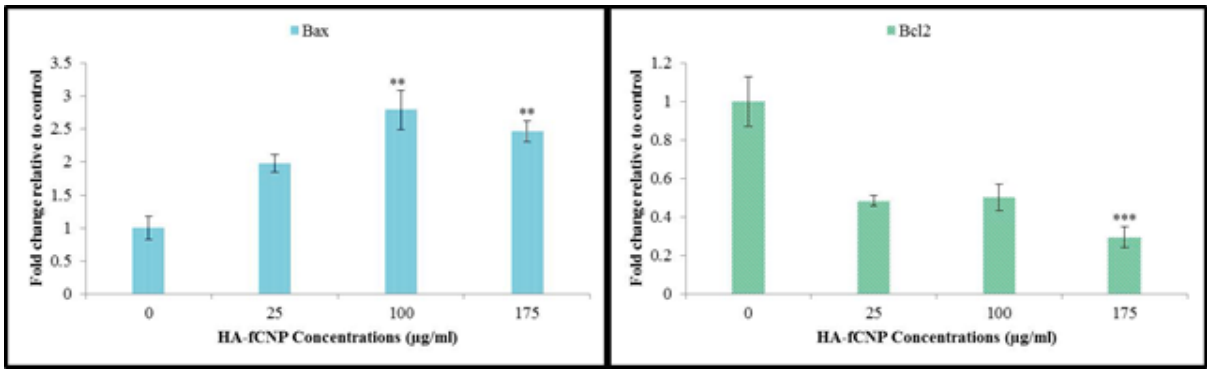


**Figure 6.** Apoptotic gene expression profile in A2780 cells following the increasing HA-fCNP treatment doses
HA-fCNP: Harmaline-ag containing folate-linked chitosan nanoparticles

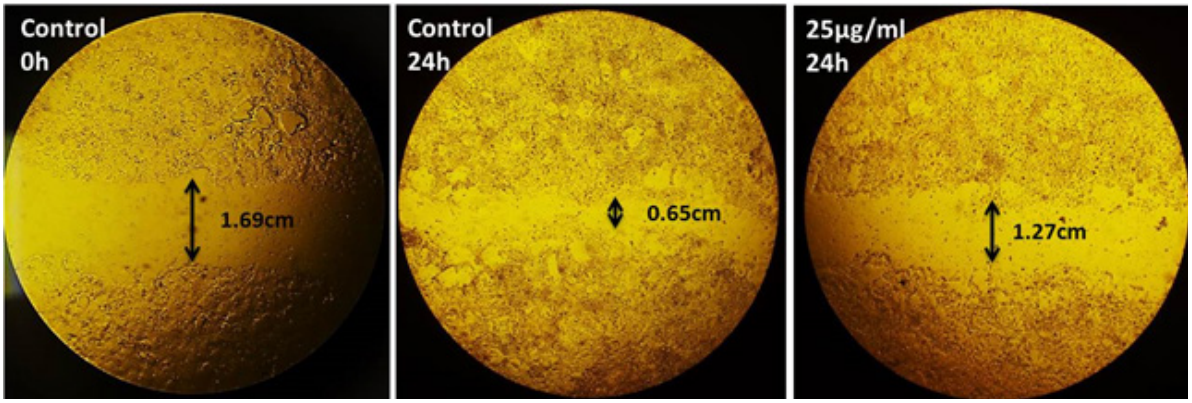


**Figure 7.** Anti-metastatic activity of HA-fCNP nanoparticles on the A2780 migration process
HA-fCNP: Harmaline-ag containing folate-linked chitosan nanoparticles

hand, the cancer cells are susceptible to an excess amount of ROS levels, which ultimately leads to their apoptotic death (35). There are several types of apoptosis inducers caused by exogenous ROS that have been found as efficient anti-ovarian cancer compounds, such as gold and silver nanoparticles (36, 37). ROS-mediated apoptosis induction is not the only mechanism the anticancer compounds have. For instance, a study reviewed the anticancer properties of turmeric curcuminoids and its other derivatives biomolecules, which have therapeutic potential in numerous chronic diseases such as colon, breast, and lung cancer (38). Also, Majumder *et al.* discussed the properties of *Aloe vera* bioactive compounds such as Aloe-emodin ((1,8-dihydroxy-3-(hydroxymethyl) anthraquinone), Aloin, Chrysophanol (1,8-dihydroxy-3-methylanthraquinone), Aloesaponarin, Acemannan, Umbelliferone (7-hydroxycoumarin), and Esculetin (6,7-dihydroxy coumarin). They showed the anti-proliferative and anti-metastatic potentials of the mentioned bioactive compounds of *Aloe vera* extract and disused their possible impacts on the most important cell growth and proliferation effector proteins including Nrf2, NF-κB, TNF-α, p53, p21, CDK1, BCL2, BAX, and cyclin B1 (39).

In this regard, harmaline has the potential to interact with mTOR signaling effectors and suppress cell growth (40). Moreover, it has been reported that harmaline acts as a potent inhibitor for sphingosine Kinase-1 (SK1)(41), which is associated with cancer development (42).

The drug delivery systems are recently designed to act as a cell-selective anticancer compound by being conjugated with cancer-associated ligands such as folic acid (43, 44). In other words, the functionalized drug delivery systems have the potential to be attached to folate receptors expressed in individual cancer cells. Therefore, their anticancer ingredients can precisely be delivered to the targeted cancer cells. Researchers successfully produced functionalized magnetic nanoparticles conjugated with Folic acid, which efficiently targeted cancer cells and released their loaded doxorubicin near them (45). Also, Wei *et al.* increased the topotecan therapeutic efficacy by producing Folic acid-conjugated mesoporous silica nanoparticles in retina cancers (46). Also, another study successfully produced a docetaxel drug delivery system consisting of a folate-conjugated lipid monolayer shell (47).

In the current study, the hybrid harmaline/silver nanoparticles were functionalized with folate-conjugated chitosan polymer to detect and target the FOLR-positive cancer cells and evaluate their apoptotic and metastatic potentials. As shown in Figure 3, the A2780 cancer cells' survival indicated greater toxicity and lower $IC_{50}$ concentration (102 µg/ml) of HA-fCNP. The PANC cancer cells' survival showed lower toxicity and greater $IC_{50}$ doses (>175 µg/ml) of HA-fCNP. This is while the HFF normal cells' survival did not change by HA-fCNP treatment doses.

HA-fCNP had been equipped with folic acid conjugations. Therefore, cells expressing folate receptor elements had more significant potential to uptake HA-fCNP through receptor-mediated endocytosis (48, 49). In other words, the significant decrease in A2780 cell survival rate following the

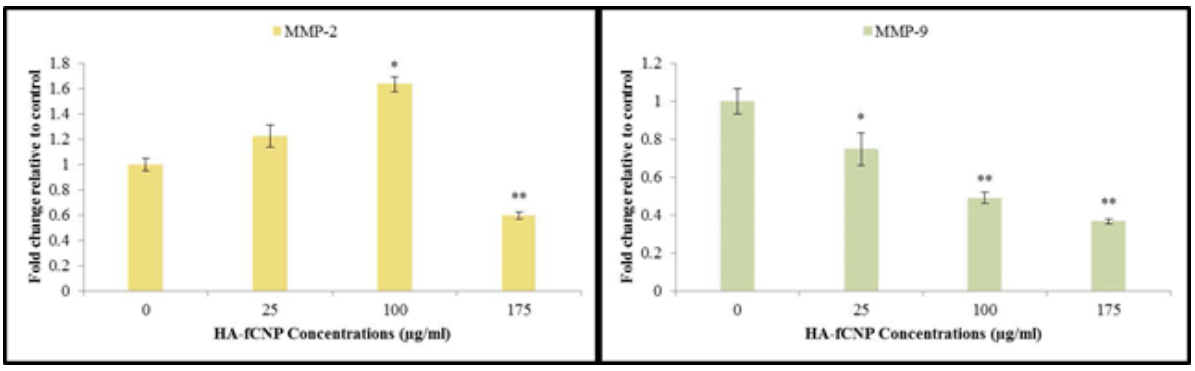


**Figure 8.** Metastatic gene expression profile in A2780 cells following the increasing HA-fCNP treatment doses
HA-fCNP: Harmaline-ag containing folate-linked chitosan nanoparticles

increasing HA-fCNP treatment doses compared with both PANC and HFF cell lines can be due to the folate receptor overexpression in A2780 cells.

Interestingly, the HA-fCNP induced apoptosis in A2780 cells by arresting them in the SubG1 phase of cell cycle status (Figure 4). This is while it was reported that harmaline and silver alone can arrest the cell cycle at the G2M phase in human gastric (SGC-7901) and lung (A549) cancer cells, respectively (50, 51). The current study shows the synergistic impact of the harmaline-silver combination on human ovarian cancer cells (A2780) can be mediated by SubG1-mediated apoptosis induction. However, evaluating the impacts of harmaline- and silver-containing folate-linked chitosan alone drug delivery systems is required to clarify the exact synergistic mechanism of HA-fCNP on A2780 cancer cell death.

## Conclusion

The results show that increasing treatment doses of HA-fCNP selectively decreased the cancer cell survival rate by inducing BAX-mediated apoptotic death and increasing the SubG1-arrested A2780 cells compared with normal HFF and cancerous PANC cells. Moreover, the high treatment doses of HA-fCNP significantly decreased A2780 metastatic ability by down-regulating MMP2/MMP9 gene expression. Therefore, HA-fCNP has the potential to be used as a safe hybrid targeted drug delivery system for ovarian cancer treatment. However, several types of *in vivo* studies are required to verify its safety and efficiency rate.

## Acknowledgment

This work was supported by Islamic Azad University, Tehran, Iran, and thus is appreciated by the author. Also, no funding was received.

## Authors' Contributions

M HT and N HR conceived and designed the research. AL WH and M HT performed the experiments and computation and wrote the main manuscript. M HT verified the analytical methods. All authors reviewed the manuscript.

## Conflicts of Interest

The authors report no conflicts of interest.

## References

1. Holmes D. Ovarian cancer: Beyond resistance. Nature 2015;527:S217.
2. Karst AM, Drapkin R. Ovarian cancer pathogenesis: A model in evolution. J Oncol 2010;2010:932371-932383.
3. Akter S, Rahman MA, Hasan MN, Akhter H, Noor P, Islam R, *et al.* Recent advances in ovarian cancer: Therapeutic strategies, potential biomarkers, and technological improvements. Cells 2022;11:650-670.
4. Chakraborti S, Ray BK, Roychoudhury S. Handbook of Oxidative Stress in Cancer: Mechanistic Aspects: Springer; 2020.
5. de Sá Junior PL, Câmara DAD, Porcacchia AS, Fonseca PMM, Jorge SD, Araldi RP, *et al.* The roles of ROS in cancer heterogeneity and therapy. Oxid Med Cell Longev 2017;2017:2467940-2467951.
6. Li X, Wang S, Mu W, Barry J, Han A, Carpenter RL, *et al.* Reactive oxygen species reprogram macrophages to suppress antitumor immune response through the exosomal miR-155-5p/PD-L1 pathway. J Exp Clin Cancer Res 2022;41:1-19.
7. Aggarwal V, Tuli HS, Varol A, Thakral F, Yerer MB, Sak K, *et al.* Role of reactive oxygen species in cancer progression: Molecular mechanisms and recent advancements. Biomolecules 2019;9:735-760.
8. Li H, Qiu Z, Li F, Wang C. The relationship between MMP-2 and MMP-9 expression levels with breast cancer incidence and prognosis. Oncol Lett 2017;14:5865-5870.
9. Quintero-Fabián S, Arreola R, Becerril-Villanueva E, Torres-Romero JC, Arana-Argáez V, Lara-Riegos J, *et al.* Role of matrix metalloproteinases in angiogenesis and cancer. Front Oncol 2019;9:1370-1390.
10. Steichen SD, Caldorera-Moore M, Peppas NA. A review of current nanoparticle and targeting moieties for the delivery of cancer therapeutics. Eur J Pharm Sci 2013;48:416-427.
11. Sawant RR, Jhaveri AM, Koshkaryev A, Zhu L, Qureshi F, Torchilin VP. Targeted transferrin-modified polymeric micelles: enhanced efficacy *in vitro* and *in vivo* in ovarian carcinoma. Mol Pharm 2014;11:375-381.
12. Wang X, Zhong X, Li J, Liu Z, Cheng L. Inorganic nanomaterials with rapid clearance for biomedical applications. Chem Soc Rev 2021;50:8669-8742.
13. Ning S, Dai X, Tang W, Guo Q, Lyu M, Zhu D, *et al.* Cancer cell membrane-coated C-TiO2 hollow nanoshells for combined sonodynamic and hypoxia-activated chemotherapy. Acta Biomater 2022;152:562-574.
14. Kalaiarasi A, Sankar R, Anusha C, Saravanan K, Aarthy K, Karthic S, *et al.* Copper oxide nanoparticles induce anticancer activity in A549 lung cancer cells by inhibition of histone deacetylase. Biotechnol Lett 2018;40:249-256.
15. Kafshdooz L, Kafshdooz T, Razban Z, Akbarzadeh A. The application of gold nanoparticles as a promising therapeutic approach in breast and ovarian cancer. Artif Cells Nanomed Biotechnol 2016;44:1222-1227.
16. Rank Miranda R, Pereira da Fonseca M, Korzeniowska B, Skytte L, Lund Rasmussen K, Kjeldsen F. Elucidating the cellular response of silver nanoparticles as a potential combinatorial agent for cisplatin chemotherapy. J Nanobiotechnology 2020;18:1-15.
17. Wang X, Li F, Yan X, Ma Y, Miao Z-H, Dong L, *et al.* Ambient aqueous synthesis of ultrasmall Ni0. 85Se nanoparticles for noninvasive photoacoustic imaging and combined photothermal-chemotherapy of cancer. ACS Appl Mater Interfaces 2017;9:41782-41793.
18. Ma Y, Wang X, Chen H, Miao Z, He G, Zhou J, *et al.* Polyacrylic acid functionalized Co0. 85Se nanoparticles: An ultrasmall pH-responsive nanocarrier for synergistic photothermal-chemo treatment of cancer. ACS Biomater Sci Eng 2018;4:547-557.
19. Phan V, Walters J, Brownlow B, Elbayoumi T. Enhanced cytotoxicity of optimized liposomal genistein via specific induction of apoptosis in breast, ovarian and prostate carcinomas. J Drug Target 2013;21:1001-1011.
20. Wang X, Ma Y, Chen H, Wu X, Qian H, Yang X, *et al.* Novel doxorubicin loaded PEGylated cuprous telluride nanocrystals for combined photothermal-chemo cancer treatment. Colloids Surf B Biointerfaces 2017;152:449-458.
21. Matthaiou E-I, Barar J, Sandaltzopoulos R, Li C, Coukos G, Omidi Y. Shikonin-loaded antibody-armed nanoparticles for targeted therapy of ovarian cancer. Int J Nanomedicine 2014;9:1855-1870.
22. Shaikh IM, Tan K-B, Chaudhury A, Liu Y, Tan B-J, Tan BM, *et al.* Liposome co-encapsulation of synergistic combination of irinotecan and doxorubicin for the treatment of intraperitoneally grown ovarian tumor xenograft. J Control Release 2013;172:852-861.
23. Guo X, Mei J, Jing Y, Wang S. Curcumin-loaded nanoparticles with low-intensity focused ultrasound-induced phase transformation as tumor-targeted and Ph-sensitive theranostic nanoplatform of ovarian cancer. Nanoscale Res Lett 2020;15:1-11.
24. Li TSC, Yawata T, Honke K. Efficient siRNA delivery and tumor accumulation mediated by ionically cross-linked folic acid-poly (ethylene glycol)–chitosan oligosaccharide lactate nanoparticles: For the potential targeted ovarian cancer gene therapy. Eur J Pharm Sci 2014;52:48-61.
25. Ganta S, Singh A, Rawal Y, Cacaccio J, Patel NR, Kulkarni P, *et al.* Formulation development of a novel targeted theranostic

nanoemulsion of docetaxel to overcome multidrug resistance in ovarian cancer. Drug Deliv 2016;23:958-970.
26. Xu B, Li M, Yu Y, He J, Hu S, Pan M, *et al*. Effects of harmaline on cell growth of human liver cancer through the p53/p21 and Fas/FasL signaling pathways. Oncol Lett 2018;15:1931-1936.
27. Abass Sofi M, Sunitha S, Ashaq Sofi M, Khadheer Pasha SK, Choi D. An overview of antimicrobial and anticancer potential of silver nanoparticles. J King Saud Univ Sci 2022;34:101791.
28. Saratale RG, Benelli G, Kumar G, Kim DS, Saratale GD. Bio-fabrication of silver nanoparticles using the leaf extract of an ancient herbal medicine, dandelion (*Taraxacum officinale*), evaluation of their antioxidant, anticancer potential, and antimicrobial activity against phytopathogens. Environ Sci Pollut Res 2018;25:10392-10406.
29. Kuppusamy P, Ichwan SJ, Al-Zikri PNH, Suriyah WH, Soundharrajan I, Govindan N, *et al*. *In vitro* anticancer activity of Au, Ag nanoparticles synthesized using *Commelina nudiflora* L. aqueous extract against HCT-116 colon cancer cells. Biol Trace Elem Res 2016;173:297-305.
30. Stetefeld J, McKenna SA, Patel TR. Dynamic light scattering: A practical guide and applications in biomedical sciences. Biophys Rev 2016;8:409-427.
31. Salopek B, Krasic D, Filipovic S. Measurement and application of zeta-potential. Rudarsko-geolosko-naftni zbornik 1992;4:147-151.
32. Chowdhury S, Basu A, Kundu S. Green synthesis of protein capped silver nanoparticles from phytopathogenic fungus *Macrophomina phaseolina* (Tassi) Goid with antimicrobial properties against multidrug-resistant bacteria. Nanoscale Res Lett 2014;9:365-375.
33. Mahmood S, Kiong KC, Tham CS, Chien TC, Hilles AR, Venugopal JR. PEGylated lipid polymeric nanoparticle-encapsulated acyclovir for *in vitro* controlled release and *ex vivo* gut sac permeation. AAPS PharmSciTech. 2020;21:1-15.
34. Azizi M, Sedaghat S, Tahvildari K, Derakhshi P, Ghaemi A. Synthesis of silver nanoparticles using Peganum harmala extract as a green route. Green Chem Lett Rev 2017;10:420-427.
35. Nakamura H, Takada K. Reactive oxygen species in cancer: Current findings and future directions. Cancer Sci 2021;112:3945-3952.
36. Fahrenholtz CD, Swanner J, Ramirez-Perez M, Singh RN. Heterogeneous responses of ovarian cancer cells to silver nanoparticles as a single agent and in combination with cisplatin. J Nanomater 2017;2017:5107485-5107504.
37. Piktel E, Ościłowska I, Suprewicz Ł, Depciuch J, Marcińczyk N, Chabielska E, *et al*. ROS-mediated apoptosis and autophagy in ovarian cancer cells treated with peanut-shaped gold nanoparticles. Int J Nanomedicine 2021;16:1993-2011.
38. Amalraj A, Pius A, Gopi S, Gopi S. Biological activities of curcuminoids, other biomolecules from turmeric and their derivatives: A review. J Tradit Complement Med 2017;7:205-233.
39. Majumder R, Das CK, Mandal M. Lead bioactive compounds of Aloe vera as potential anticancer agent. Pharmacol Res 2019;148:104416.
40. Zhang Y, Shi X, Xie X, Laster KV, Pang M, Liu K, *et al*. Harmaline isolated from *Peganum harmala* suppresses growth of esophageal squamous cell carcinoma through targeting mTOR. Phytother Res Phytother Res 2021;35:6377-6388.
41. Roy S, Mohammad T, Gupta P, Dahiya R, Parveen S, Luqman S, *et al*. Discovery of harmaline as a potent inhibitor of sphingosine kinase-1: A chemopreventive role in lung cancer. ACS Omega 2020;5:21550-21560.
42. Ogretmen B, Hannun YA. Biologically active sphingolipids in cancer pathogenesis and treatment. Nat Rev Cancer 2004;4:604-616.
43. Farran B, Montenegro RC, Kasa P, Pavitra E, Huh YS, Han YK, *et al*. Folate-conjugated nanovehicles: Strategies for cancer therapy. Mater Sci Eng C Mater Biol Appl 2020;107:110341.
44. He G, Ma Y, Zhou H, Sun S, Wang X, Qian H, *et al*. Mesoporous NiS 2 nanospheres as a hydrophobic anticancer drug delivery vehicle for synergistic photothermal-chemotherapy. J Mater Chem B 2019;7:143-149.
45. Andhariya N, Upadhyay R, Mehta R, Chudasama B. Folic acid conjugated magnetic drug delivery system for controlled release of doxorubicin. J Nanopart Res 2013;15:1-12.
46. Qu W, Meng B, Yu Y, Wang S. Folic acid-conjugated mesoporous silica nanoparticles for enhanced therapeutic efficacy of topotecan in retina cancers. Int J Nanomedicine 2018;13:4379-4389.
47. Liu Y, Li K, Pan J, Liu B, Feng SS. Folic acid conjugated nanoparticles of mixed lipid monolayer shell and biodegradable polymer core for targeted delivery of Docetaxel. Biomaterials 2010;31:330-338.
48. Carron PM, Crowley A, O'Shea D, McCann M, Howe O, Hunt M, *et al*. Targeting the folate receptor: Improving efficacy in inorganic medicinal chemistry. Curr Med Chem 2018;25:2675-2708.
49. Seyedi SMR, Asoodeh A, Darroudi M. The human immune cell simulated anti-breast cancer nanorobot: The efficient, traceable, and dirigible anticancer bio-bot. Cancer Nanotechnol 2022;13:1-24.
50. Wang Y, Wang C, Jiang C, Zeng H, He X. Novel mechanism of harmaline on inducing G2/M cell cycle arrest and apoptosis by up-regulating Fas/FasL in SGC-7901 cells. Sci Rep2015;5:18613-18622.
51. Lee YS, Kim DW, Lee YH, Oh JH, Yoon S, Choi MS, *et al*. Silver nanoparticles induce apoptosis and G2/M arrest via PKCζ-dependent signaling in A549 lung cells. Arch Toxicol 2011;85:1529-1540.